Tailoring Fe-doped Co_3O_4 Nanoparticles via Ultrasonic Cell Disruption: Mechanistic Insights and High-Performance Alkaline HER Electrocatalysts

Mutian Zhang [a,1], Ziying Ji [b, 1], Shijie Pan [b], Xiang Liu [a], Wei Zheng [a], Jiajia Wang [b, *], Guobing Ying [a, *]

a: School of Materials Science and Engineering, Southeast University, Nanjing, Jiangsu, 211189, China

b: College of Materials Science and Engineering, Hohai University, Nanjing, Jiangsu, 210098, China

1: The authors contribute equally to this work.

Supplementary Information

Table S1. Hubbard U values of transition metal elements.

Elements	U values (eV)	Ref.
Co	4.7	Our previous work
Fe	4.0	[1]

The Conjugate Gradient (CG) geometric optimization algorithm was used until the force per atom was less than 0.02 eV / Å and the energy gap was less than $1*10^{-5}$ eV / atom until final convergence[2].

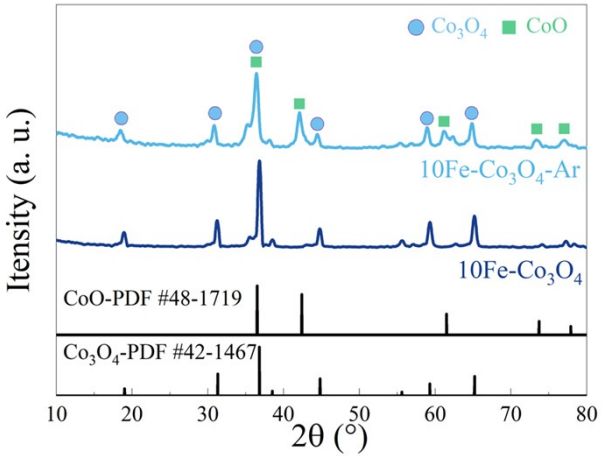

Figure S1 XRD patterns of different annealing conditions of 10Fe-Co_3O_4(Co_3O_4: JCPDS No. 42-1467, CoO: JCPDS No. 48-1719).

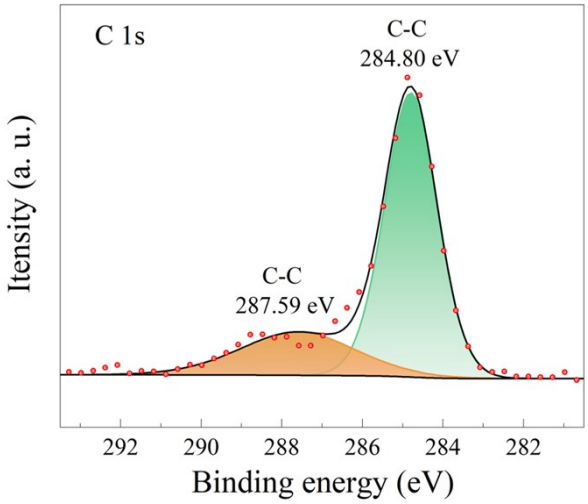

Figure S2 XPS spectra of 10Fe-Co_3O_4 of C 1s for charge correction.

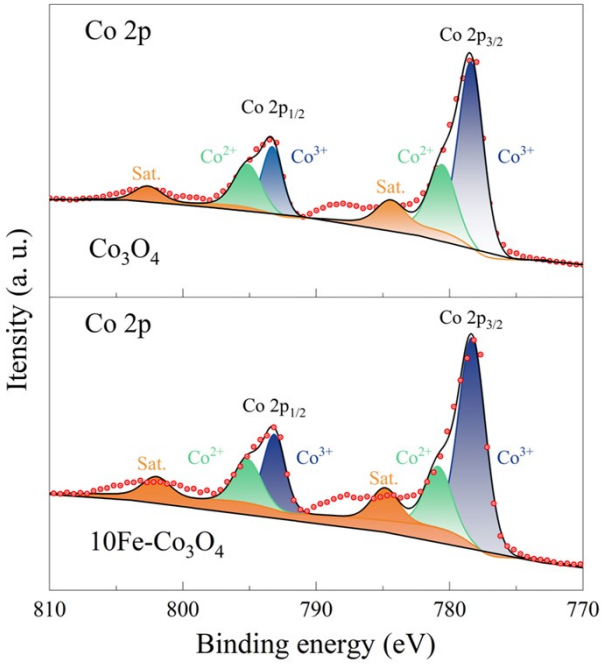

Figure S3 XPS spectra of Co_3O_4 and 10Fe-Co_3O_4 of Co 2p.

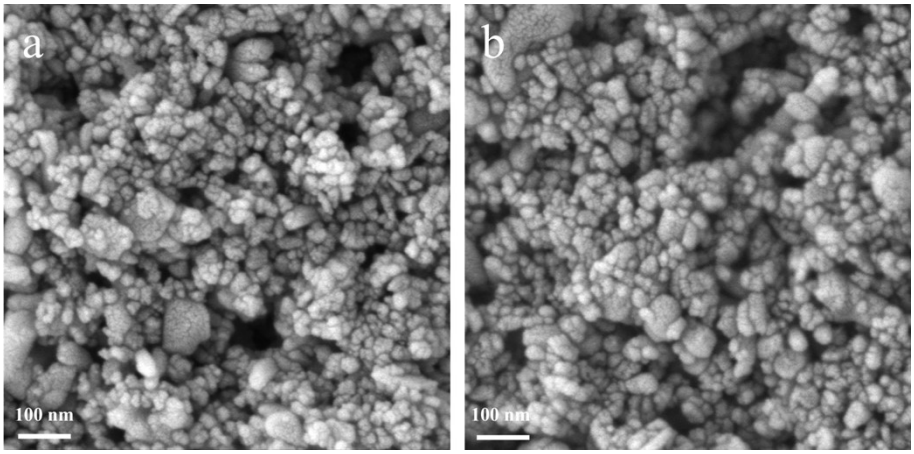

Figure S4 SEM images of 10Fe-Co_3O_4 UNPs prepared under different sonication conditions: a) 2 h treatment, (b) 4 h treatment.

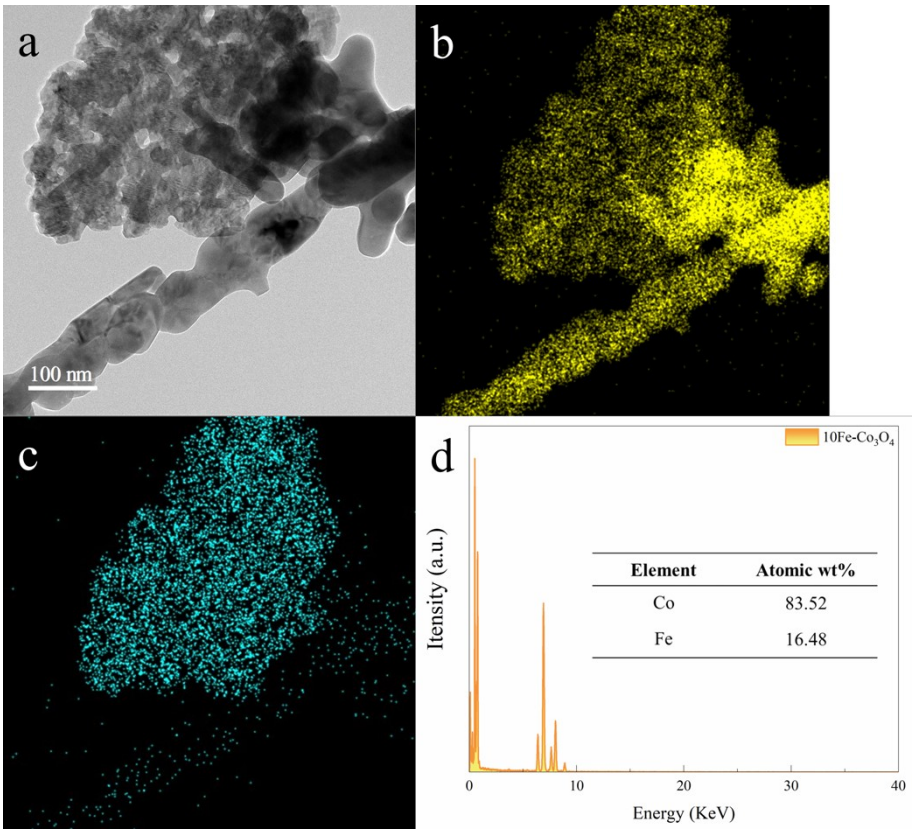

Figure S5 (a)TEM image of 10Fe-Co_3O_4 UNPs and TEM element mapping of Co (b), Fe (c), and EDS diagram of 10Fe-Co_3O_4 UNPs.

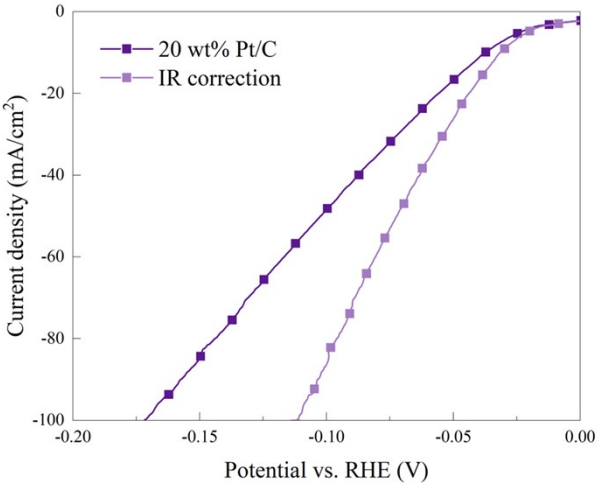

Figure S6 LSV curves and IR-correction of Pt/C commercial catalysts (Pt 20 wt.%). $\eta 10$ = 37.7 mV, which is similar to the value of references[3].

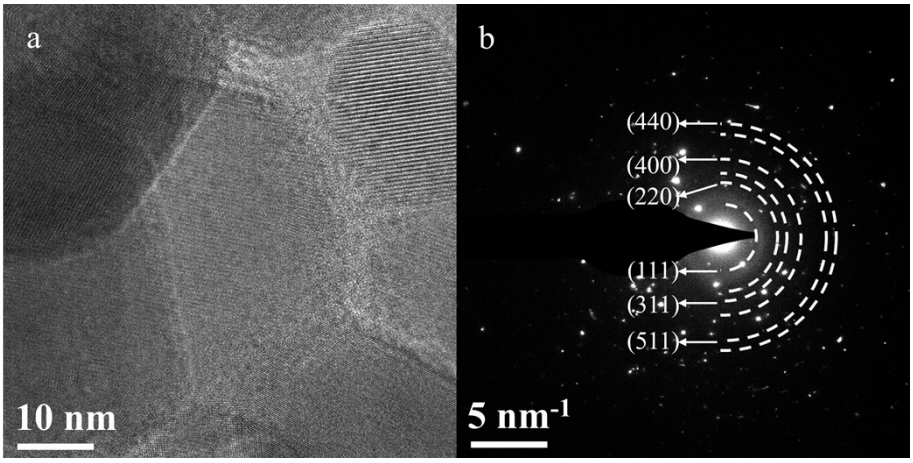

Figure S7. (a) HRTEM image and (b) SAED pattern of 10Fe-Co_3O_4 UNPs after a 24-hour durability test at a current density of 100 mA/cm^2. The observed diffraction rings in (b) originate from the conductive carbon powder and binder introduced during catalyst ink preparation.

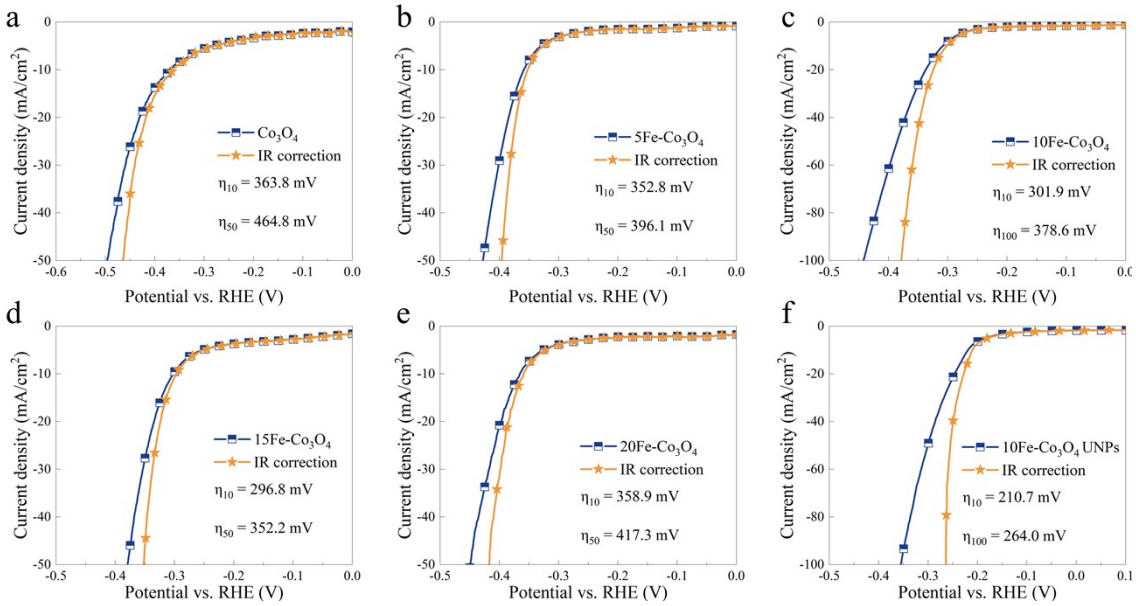

Figure S8 LSV curves and IR-correction of Co_3O_4 (a), 5Fe-Co_3O_4 (b), 10Fe-Co_3O_4 (c), 15Fe-Co_3O_4 (d), 20Fe-Co_3O_4 (e), and 10Fe-Co_3O_4 UNPs (f).

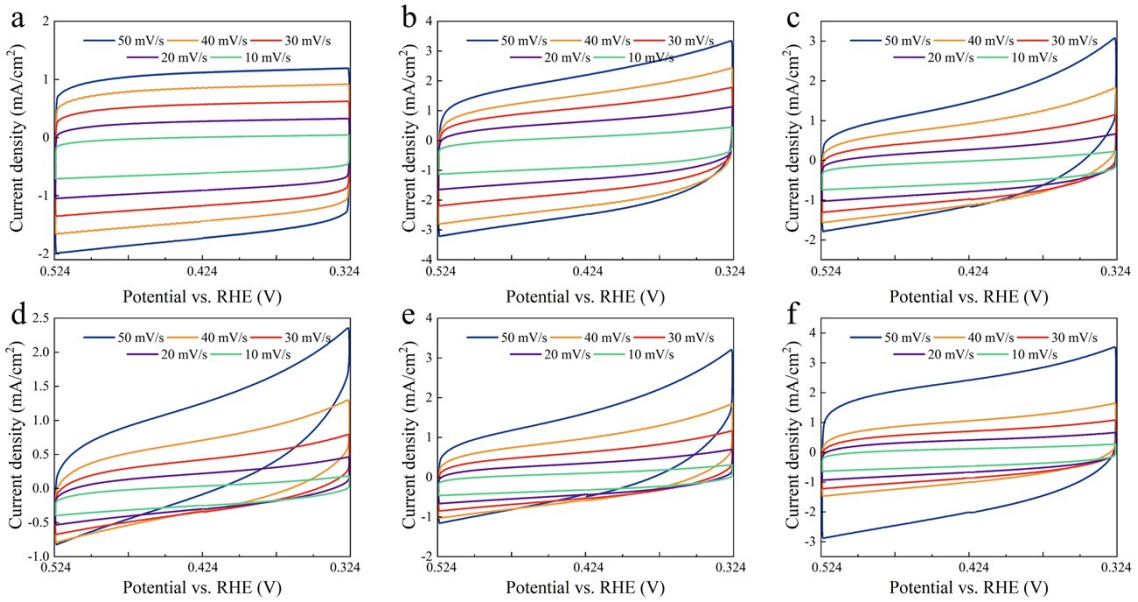

Figure S9 CV curves of Co_3O_4 (a), 5Fe-Co_3O_4 (b), 10Fe-Co_3O_4 (c), 15Fe-Co_3O_4 (d), 20Fe-Co_3O_4 (e), and 10Fe-Co_3O_4 UNPs (f).

To investigate the influence of Fe doping on the catalytic properties of the Co_3O_4 (220) surface, we have expanded our DFT calculations to include a broader range of Fe doping concentrations. Specifically, we now consider five doping levels: undoped (0%) and doping ratios of 5%, 10%, 15%, and 20%, resulting in a total of 11 models, and the 10 doped models are shown in Fig. S9.

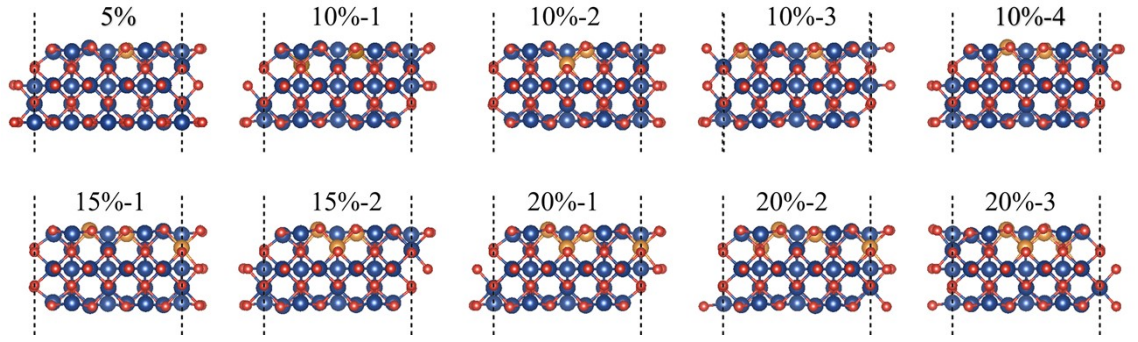

Figure S10 Side view of 10 different Fe-doping ratio (220) surface models of Co_3O_4.

For these models, we calculated both the formation energies and the water adsorption energies on their surfaces. The formation energy (E_{form}) for Fe doping in Co_3O_4 is calculated as:

$$E_{form} = \frac{1}{n}\left[E_{SlabFe-Co_3O_4} - E_{SlabCo_3O_4} + n\mu_{Co} - n\mu_{Fe}\right] \quad (1)$$

Where $E_{SlabFe-Co_3O_4}$ is defined as the total energy of the Fe-Co3O4 slab, $E_{SlabCo_3O_4}$ is defined as the total energy of the Co_3O_4 slab, n is the number of substituted Fe atoms, μ_{Co} and μ_{Fe} are the chemical potential of Co and Fe, calculated by their bulk free energy.

The adsorption energy(E_{ads}) is defined as[4]:

$$E_{ads} = E_{slab@H_2O} - [E_{slab} + E_{H_2O}] \quad (2)$$

Where $E_{slab@H_2O}$, E_{slab} and E_{H_2O} represent the total energy of the system after the adsorption of water molecules, the energy of the system before the adsorption of water molecules and the energy of the water molecules, respectively. The absolute value of E_{ads} signifies the adsorption capacity of this adsorption behaviour of the system for water molecules. The corresponding data are provided in Table S2.

Table S2 The formation energy (eV) and adsorption energy (eV) of different Fe-doping ratio structures.

Structure	E_{form} (eV)	E_{ads} (eV)
0%	0	-2.18
5%	0.68	-2.73
10%-1	3.17	-2.65
10%-2	2.80	-2.76
10%-3	3.12	-2.84
10%-4	3.26	-3.05
15%-1	3.51	-2.98
15%-2	3.48	-2.99
20%-1	4.22	-3.01
20%-2	5.70	-3.10
20%-3	6.10	-3.05

To facilitate a more intuitive comparison, we have also presented the results graphically in Fig. S10. As illustrated, with increasing doping concentration, the formation energy rises, indicating that higher doping concentrations make the material harder to synthesize. At the same time, the water adsorption energy decreases, suggesting that higher doping concentrations are more favourable for water adsorption.

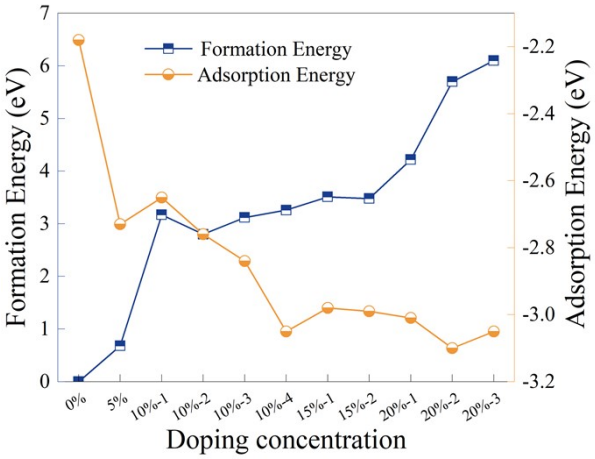

Figure S11 The formation energy and adsorption energy of different Fe-doping ratio structures.

The increasing formation energy and decreasing adsorption energy present a trade-off, implying that an optimal doping concentration is necessary. Based on the results from Fig. S10, we find that doping concentrations of 5% and 10% strike a good balance between ease of doping and water adsorption capability. Among these, we specifically chose the 10%-4 model for further analysis, as it exhibited the strongest water adsorption energy within the 10% doping group while maintaining a formation energy close to that of other models at this doping level. This makes the 10%-4 model particularly promising for HER applications, as it provides a good balance between water adsorption efficiency and doping feasibility. Therefore, we focus on these two doping levels in the main manuscript, where we refer to them as Single-Fe Co_3O_4 (5%) and Double-Fe Single-Fe Co_3O_4 (10%-4) for further calculation.

Table S3 Average Bader charge population (|e|) of surface-active sites on the (220) surface of Co_3O_4, Single Fe-Co_3O_4 and Double Fe-Co_3O_4.

System	Co^{3+}	Fe^{3+}	O
Co_3O_4	7.902	/	6.928

Single Fe-Co_3O_4	7.850	6.590	7.035
Double Fe-Co_3O_4	7.820	6.455	7.075

Table S4 Average Bader charge transfer (|e|) of surface-active sites on the (220) surface of Co_3O_4, Single Fe-Co_3O_4 and Double Fe-Co_3O_4.

System	Co^{3+}	Fe^{3+}	O
Co_3O_4	+1.098	/	-0.928
Single Fe-Co_3O_4	+1.150	+1.410	-1.035
Double Fe-Co_3O_4	+1.180	+1.545	-1.075

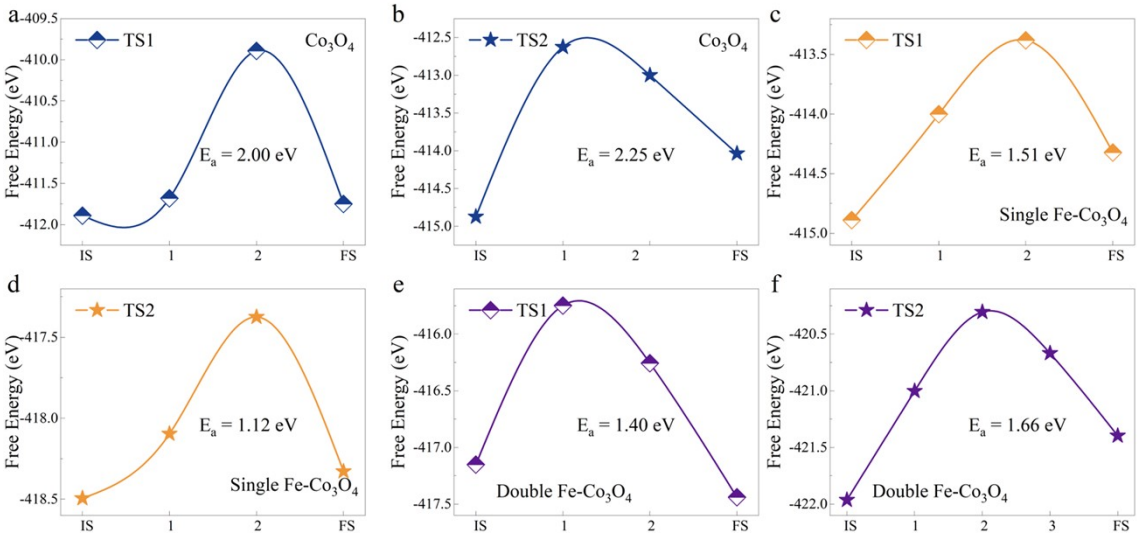

Figure S12 (a)(b) The two step energy barriers of water splitting on the (220) surface of Co_3O_4; (c)(d) The two step energy barriers of water splitting on the (220) surface of Single Fe-Co_3O_4; (e)(f) The two step energy barriers of water splitting on the (220) surface of Double Fe-Co_3O_4.

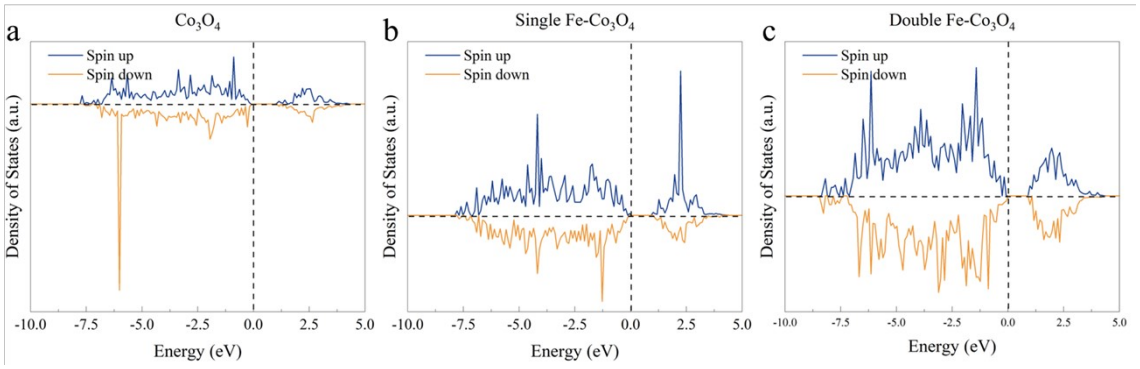

Figure S13 The total density of states of the (220) surface of Co_3O_4 (a), Single Fe-Co_3O_4 (b) and Double Fe-Co_3O_4 (c).

ε_d are obtained by Vaspkit software[5].

References

1. P. Yoo and P. Liao, *Appl. Surf. Sci.*, 2023, **630**, 157501.
2. Y. Cao, K.-C. Leung and V. O. K. Li, *Ieee Transactions on Wireless Communications*, 2008, **7**, 2094-2105.
3. L. Hou, Z. Li, H. Jang, M. G. Kim, J. Cho, W. Zhong, s. Liu and X. Liu, *Angew. Chem., Int. Ed.*, 2024, e202423756.
4. J. Chen and A. Selloni, *The Journal of Physical Chemistry Letters*, 2012, **3**, 2808-2814.
5. V. Wang, N. Xu, J.-C. Liu, G. Tang and W.-T. Geng, *Comput. Phys. Commun.*, 2021, **267,** 108033.